

# Two-dimensional retrieval methods for ultrafast imaging of molecular structure using laser-induced electron diffraction

Cite as: J. Chem. Phys. **155**, 164104 (2021); <https://doi.org/10.1063/5.0064761>

Submitted: 27 July 2021 • Accepted: 04 October 2021 • Accepted Manuscript Online: 04 October 2021 • Published Online: 25 October 2021

 Su-Ju Wang,  Jiří Daněk, Cosmin I. Blaga, et al.



View Online



Export Citation



CrossMark

## ARTICLES YOU MAY BE INTERESTED IN

[A unified and flexible formulation of molecular fragmentation schemes](#)

The Journal of Chemical Physics **155**, 164105 (2021); <https://doi.org/10.1063/5.0059598>

[Solving the Schrödinger equation using program synthesis](#)

The Journal of Chemical Physics **155**, 154102 (2021); <https://doi.org/10.1063/5.0062497>

[Advanced x-ray spectroscopy of actinide trichlorides](#)

The Journal of Chemical Physics **155**, 164103 (2021); <https://doi.org/10.1063/5.0062927>



Webinar  
Quantum Material Characterization  
for Streamlined Qubit Development



Register now

# Two-dimensional retrieval methods for ultrafast imaging of molecular structure using laser-induced electron diffraction

Cite as: *J. Chem. Phys.* **155**, 164104 (2021); doi: [10.1063/5.0064761](https://doi.org/10.1063/5.0064761)

Submitted: 27 July 2021 • Accepted: 4 October 2021 •

Published Online: 25 October 2021



View Online



Export Citation



CrossMark

Su-Ju Wang,<sup>1,a)</sup> Jiří Daněk,<sup>1</sup> Cosmin I. Blaga,<sup>1</sup> Louis F. DiMauro,<sup>2</sup> Jens Biegert,<sup>3,4</sup> and C. D. Lin<sup>1,b)</sup>

## AFFILIATIONS

<sup>1</sup>J. R. Macdonald Laboratory, Department of Physics, Kansas State University, Manhattan, Kansas 66506, USA

<sup>2</sup>Department of Physics, The Ohio State University, Columbus, Ohio 43210, USA

<sup>3</sup>ICFO-Institut de Ciències Fòniques, The Barcelona Institute of Science and Technology, 08860 Castelldefels, Barcelona, Spain

<sup>4</sup>Institució Catalana de Recerca i Estudis Avançats (ICREA), Pg. Lluís Companys 23, 08010 Barcelona, Spain

<sup>a)</sup> Author to whom correspondence should be addressed: [sjwang@phys.ksu.edu](mailto:sjwang@phys.ksu.edu)

<sup>b)</sup> [cdlin@phys.ksu.edu](mailto:cdlin@phys.ksu.edu)

## ABSTRACT

Molecular structural retrieval based on electron diffraction has been proposed to determine the atomic positions of molecules with sub-angstrom spatial and femtosecond temporal resolutions. Given its success on small molecular systems, in this work, we point out that the accuracy of structure retrieval is constrained by the availability of a wide range of experimental data in the momentum space in all molecular systems. To mitigate the limitations, for laser-induced electron diffraction, here we retrieve molecular structures using two-dimensional (energy and angle) electron momentum spectra in the laboratory frame for a number of small molecular systems, which have previously been studied with 1D methods. Compared to the conventional single-energy or single-angle analysis, our 2D methods effectively expand the momentum range of the measured data. Besides utilization of the 2D data, two complementary methods are developed for consistency check on the retrieved results. The 2D nature of our methods also offers a way of estimating the error from retrieval, which has never been explored before. Comparing with results from prior experiments, our findings show evidence that our 2D methods outperform the conventional 1D methods. Paving the way to the retrieval of large molecular systems, in which their tunneling ionization rates are challenging to obtain, we estimate the error of using the isotropic model in place of including the orientation-dependent ionization rate.

Published under an exclusive license by AIP Publishing. <https://doi.org/10.1063/5.0064761>

## I. INTRODUCTION

Ultrafast imaging of time-resolved atomic motions in molecules is a prerequisite to disentangle the complex pathways during a chemical reaction. Such investigation in the laboratories had not been possible because of the challenge of developing experimental tools that can achieve sub-angstrom spatial resolutions and femtosecond to sub-femtosecond temporal resolutions. With the development of intense ultrafast lasers as well as the national accelerator-based free-electron light sources<sup>1–3</sup> over the past decade, light pulses with a duration of few femtoseconds or even attoseconds have become available. These light sources have been used in ultrafast absorption or emission spectroscopy for

probing ultrafast chemical dynamics, yet spectroscopic information is difficult to interpret if the conformational arrangement of atoms in the molecules is not known, which is certainly the case when molecules are under transformation.

For gas-phase molecules in their ground states, electron diffraction by high-energy electrons (above hundreds of keV) is a well-established method of probing the interatomic separations in molecules. While ultrafast electron diffraction (UED) has existed since the 1990s,<sup>4,5</sup> compressing electron pulses down to tens of femtoseconds has not yet been possible until the present day. Recent progress at laboratories using tens or hundreds of keV electrons has achieved sub-picosecond pulses.<sup>6–8</sup> Using 2–4 MeV high-energy electrons, pulses as short as 100 fs have become available and

successfully used to carry out a number of ultrafast MeV-UED experiments.<sup>9–12</sup> With increasing efforts in many laboratories, UED is expected to make steady progress toward sub-100 fs duration, but how quickly it can be reached remains an open question.

An alternative tool for achieving ultrafast dynamic imaging of molecules is the so-called laser-induced electron diffraction (LIED).<sup>13,14</sup> Instead of using electrons generated by external sources, in LIED, the diffraction images are generated by electrons from the molecule itself. When an intense laser impinges on a molecule, the strong electric field near the peak of the optical cycle is capable of ripping off electrons from molecules' outer shells. A fraction of these field-ionized electrons would be driven back, when the laser's electric field reverses its direction, to collide with the molecular ions left behind and emerge carrying the structural information of the target analogous to electron scattering of molecules in conventional electron diffraction (CED). Thus, the basic underlying principle of LIED is simple and the concept has been already addressed in 1993.<sup>15</sup> Regardless of the similarity between these two imaging methods, there are two obstacles in treating LIED as CED. First of all, since, in LIED, electron scattering occurs in the presence of an intense laser field, it was not obvious how the diffraction images would be modified by the external field. Second, electron energies in typical CED are over 100 keV, while in typical Ti:sapphire 800-nm lasers, the electron rescattering energies are only in the range of a few tens of eV. At such low energies, the differential cross sections (DCSs) carry information about valence electrons, and thus, it is almost impossible to unravel the DCS to retrieve bond lengths.

Successfully, these two questions have been addressed in previous theoretical studies.<sup>16–18</sup> For one, quantitative rescattering (QRS) theory<sup>19–21</sup> offers an elegant way to isolate the effect of the external field and thus allows field-free elastic electron scattering differential cross sections to be retrieved directly from the high-energy photoelectron spectra. Second, to probe molecular bond lengths, one does not have to use 100 keV electrons if the accuracy of bond lengths within about 0.05 Å (5 pm) is acceptable (instead of picometers in CED). In such cases, as shown in the work of Xu *et al.*,<sup>18</sup> rescattering electrons with energies from about 50 to a few hundreds of electron volts will be enough if the photoelectron images are taken at large scattering angles, which were due to collision events at small impact parameters. Such scattering undergoes the same momentum transfer as CED using hundreds of keV electrons with images taken at small angles.

In the work of Xu *et al.*,<sup>18</sup> it was established that LIED is capable of achieving sub-angstrom spatial resolution if mid-infrared (MIR) lasers with wavelength near and above 2000 nm are used. In the work of Blaga *et al.*,<sup>22</sup> using MIR lasers, LIED was first employed to image the bond lengths of simple diatomic molecules as N<sub>2</sub> and O<sub>2</sub>, with spatial resolution within 0.05 Å. Subsequently, 3.2- $\mu$ m lasers were used to study more complex molecules, such as C<sub>2</sub>H<sub>2</sub>,<sup>23,24</sup> CS<sub>2</sub>,<sup>25</sup> H<sub>2</sub>O,<sup>26</sup> NH<sub>3</sub>,<sup>27</sup> and OCS<sup>28</sup> molecules in their ground states. Other laboratories have also reported some LIED experiments using wavelengths slightly shorter than 2.0  $\mu$ m.<sup>29,30</sup>

In CED or LIED, to retrieve bond length information from the electron momentum spectra, only diffraction images originating from close collisions with the constituent atoms are useful. With given diffraction images, reconstruction of molecular structures is still nontrivial. For CED, the retrieval is based on the Fourier

transform (FT) or using the so-called independent-atom model (IAM).<sup>31–33</sup> The former is straightforward and parameter-free but would require a large range of momentum transfer in the scattering data to separate out closely spaced bond lengths. The latter is based on an iterative fitting procedure by matching the measured finite momentum-range data with the predicted values in a parameter space formed by bond lengths. The solution is intrinsically non-unique since one is trying to create entire-momentum-range knowledge based on existing finite momentum-range information from experiments (called the finite momentum-range problem throughout the paper). If the available range is not sufficient, one could end up having multiple competitive solutions, leading to an inconclusive result. Another issue is that the iterating fitting uses the least squares fitting that is not democratic as it puts more weight on the larger amplitude parts than the smaller ones, leading to potential errors. To extract transient molecular structures from electron diffraction images, irrespective of their origins, whether they are from photoelectron momentum spectra generated by MIR lasers or from MeV high-energy beams, efficient and reliable retrieval methods continue to pose challenges.

All the existing LIED-based retrieval methods are built upon the extraction of field-free DCS in the laser polarization frame. By analyzing oscillation embedded in the DCS, the so-called molecular contrast factor (MCF), as a function of momentum transfer for either a fixed rescattering energy or a fixed rescattering angle, molecular bond lengths are retrieved. The former fixed-energy approach<sup>18,22,23,29,30,34</sup> does not have a particular name and is commonly referred to as LIED. In this approach, one searches for the bond lengths by iteratively fitting the overall shape of MCF given by IAM and uses the sum of squares of errors as the fitness function in the optimization process; for clarity, we term this method as the standard LIED (SD-LIED). The latter is named as fixed-angle broadband laser-driven electron scattering (FABLES)<sup>35</sup> and has been done mostly at  $\theta_r = 180^\circ$ . FABLES relies on the inverse Fourier transform to reconstruct the molecular structures and thus is also called FT-LIED lately.

These types of laser-frame analyses, such as in SD-LIED and FT-LIED, involve one extra step of manipulating the experimental data, that is, a transformation from the laboratory frame to the laser polarization frame. To circumvent this laborious process, in this work, we propose to analyze the experimental photoelectron spectra directly in the laboratory frame. In addition, we go beyond the previous one-energy or one-angle analysis by extracting two-dimensional DCSs directly in the laboratory frame covering a certain range of the detected electron momentum and the laboratory-frame scattering angle. The latter takes advantage of the special feature of LIED, i.e., the electron beam generating diffraction images is a broadband, unlike the monochromatic electron beam in conventional high-energy field-free electron diffraction. This is the very first time that this feature is implemented in the structural retrieval and systematically examined.

The rest of this article is arranged as follows: In Sec. II, we first review the basic principle and relevant mathematical expressions governing the LIED method and summarize the existing LIED-based methods of retrieving molecular bond lengths. Then, we illustrate our new method with the example of O<sub>2</sub> retrieval. After such a procedure is demonstrated, our new method is applied to

reanalyze prior experiments and retrieve bond lengths. The results are discussed in Sec. III. Finally, we conclude our work in Sec. IV.

## II. THEORY AND METHODS

### A. QRS model and photoelectron spectra

According to the QRS model,<sup>36</sup> for a spaced-fixed molecule (denoting the orientation angles of the molecule as  $\Omega_L$ ), the high-energy photoelectron distribution  $I(\mathbf{k}, \Omega_L)$  in the  $[2U_p, 10U_p]$  rescattering range, where  $U_p$  is the ponderomotive energy, can be decomposed into two parts,

$$I(\mathbf{k}, \Omega_L) = W(k_r, \Omega_L) \times \sigma(\mathbf{k}_r, \Omega_L), \quad (1)$$

where  $W(k_r, \Omega_L)$  is the momentum distribution of the returning electrons and  $\sigma(\mathbf{k}_r, \Omega_L)$  is the field-free elastic differential cross section of the target molecular ion scattered by an incident electron with energy  $E_r = k_r^2/2$ . Atomic units are used throughout this article unless otherwise stated. The vector  $\mathbf{k} = \{k, \theta_k, \phi_k\}$  is the measured electron's momentum in the laboratory frame, and  $\mathbf{k}_r = \{k_r, \theta_r, \phi_r\}$  is the electron's momentum in the laser polarization frame. These two vectors are represented in the spherical coordinates with the laser polarization as the  $z$  axis. Since the electron is scattered in the presence of the external field, it gains an additional momentum kick  $-\mathbf{A}_r = -\mathbf{A}(t_r)$  from the vector potential  $\mathbf{A}$  of the laser field at the return time  $t_r$  after exiting the field. Therefore, these two momenta are related by

$$\mathbf{k} = -\mathbf{A}_r + \mathbf{k}_r. \quad (2)$$

These quantities  $t_r$ ,  $\mathbf{k}_r$ , and  $\mathbf{A}_r$  could be calculated using the classical theory.<sup>15,16,18,37</sup> The relation in Eq. (2) is similar to the one transforming a particle's velocity between the laboratory frame of reference and the center-of-mass frame in classical mechanics.

The returning electron distribution term  $W(k_r, \Omega_L)$  can be further broken down into

$$W(k_r, \Omega_L) = w_{\text{TI}}(\Omega_L) \times \tilde{W}(k_r), \quad (3)$$

where the orientation dependence is attributed to the tunneling ionization rate  $w_{\text{TI}}(\Omega_L)$  of the molecules. Thus, we arrive at

$$I(\mathbf{k}, \Omega_L) = \tilde{W}(k_r) \times w_{\text{TI}}(\Omega_L) \times \sigma(\mathbf{k}_r, \Omega_L). \quad (4)$$

For long-wavelength lasers used for the LIED experiments, the electron distribution has a weak energy dependence,<sup>16</sup> so the factor  $\tilde{W}(k_r)$  can be disregarded. In this case, the DCS in the laboratory frame  $I$  can be calculated directly by transforming the DCS in the laser polarization frame  $\sigma$  with the relation in Eq. (2).

### B. IAM and structural retrieval

Calculations of the elastic differential cross sections for field-free electron-molecule collisions are, in general, quite complicated. However, for high energies, scattering occurs only near the center of each atom in the molecule, where chemical bondings and electron correlation are insignificant, and thus, the molecule can be approximated by a collection of non-interacting atoms, meaning we can apply the independent-atom model to calculate the differential cross sections. In IAM, the potential seen by the incident electron is approximated by the sum of the potential from the individual atoms. Therefore, the scattering amplitude for an electron with an

initial momentum  $\mathbf{k}_{r,0}$  and a final momentum  $\mathbf{k}_r$  after colliding with a fixed-in-space molecule can be written as

$$F(\mathbf{k}_r, \Omega_L) = \sum_{\alpha=1}^N f_{\alpha} e^{i(\mathbf{k}_r - \mathbf{k}_{r,0}) \cdot \mathbf{R}_{\alpha}} = \sum_{\alpha=1}^N f_{\alpha} e^{i\mathbf{q} \cdot \mathbf{R}_{\alpha}}, \quad (5)$$

where  $N$  is the total number of atoms in the molecule,  $f_{\alpha}$  is the scattering amplitude of the electron with the  $\alpha$ th atom located in the coordinate of  $\mathbf{R}_{\alpha}$ , and  $\mathbf{q} \equiv \mathbf{k}_r - \mathbf{k}_{r,0}$  is the momentum transfer of electrons. The information of the atomic positions is imprinted in the phase factor contributing to the final scattering amplitude  $F$ . Since the fixed-in-space molecule has an orientation, which is generally different from that of the laboratory coordinate system, the final scattering amplitude would thus depend on the orientation angles of molecules labeled by  $\Omega_L$ . For an elastic collision (i.e.,  $|\mathbf{k}_r| = |\mathbf{k}_{r,0}| = k_r$ ), the momentum transfer  $\mathbf{q}$  has a magnitude of  $q = 2k_r \sin(\theta_r/2)$ , assuming that the incident electron is along the  $z$  direction. The absence of the  $\phi_r$  dependence is a result of cylindrical symmetry.

With the scattering amplitude in Eq. (5), the electron-molecular scattering differential cross section is then given by the modulus square of the total amplitude as

$$\sigma(\mathbf{k}_r, \Omega_L) = \sum_{\alpha=1}^N |f_{\alpha}|^2 + \sum_{\alpha=1}^N \sum_{\beta \neq \alpha}^N f_{\alpha} f_{\beta}^* e^{i\mathbf{q} \cdot (\mathbf{R}_{\alpha} - \mathbf{R}_{\beta})}. \quad (6)$$

The first term on the right-hand side of Eq. (6) is called the atomic term,  $\sigma_A \equiv \sum_{\alpha=1}^N |f_{\alpha}|^2$ , which is an incoherent sum of the scattering between the electron and the individual atoms. The second term is called the molecular interference term (MIT) or  $\sigma_M$ , which encodes the structural information of molecules and thus is the key to LIED. Sometimes, it is useful to look at the molecular contrast factor (MCF) or  $\gamma_C$ , which is defined by  $\gamma_C = \sigma_M/\sigma_A$  and is typically of the order of few to 15%.

If the molecular gas has a certain spatial distribution or one wants to take the tunneling ionization rate into account, averaging over the angular dependence of the alignment distribution/the ionization rate is necessary. The three-dimensional average integral is

$$\bar{\sigma}(\mathbf{k}_r) = \sum_{\alpha=1}^N |f_{\alpha}|^2 + \sum_{\alpha=1}^N \sum_{\beta \neq \alpha}^N f_{\alpha} f_{\beta}^* \frac{\int e^{i\mathbf{q} \cdot (\mathbf{R}_{\alpha} - \mathbf{R}_{\beta})} \rho(\Omega_L) \omega_{\text{TI}}(\Omega_L) d\Omega_L}{\int \rho(\Omega_L) \omega_{\text{TI}}(\Omega_L) d\Omega_L}, \quad (7)$$

where the orientation dependence of the molecular axis is expressed by the three Euler angles  $\Omega_L = \{\theta_L, \phi_L, \chi_L\}$  with respect to the polarization direction of the laser beam, the function  $\rho(\Omega_L)$  is the angular distribution of the molecules, and  $\omega_{\text{TI}}(\Omega_L)$  is the tunneling ionization rate. The angular distribution  $\rho(\Omega_L)$  can be obtained from experiments or some theoretical model,<sup>36</sup> while  $\omega_{\text{TI}}(\Omega_L)$  can be obtained from the molecular Ammosov-Delone-Krainov (MO-ADK) theory.<sup>38</sup>

Including angular distribution and tunneling ionization rate requires more computational efforts. If the molecules are randomly oriented and the alignment dependence of the ionization rate is neglected [i.e.,  $\rho(\Omega_L) = \omega_{\text{TI}}(\Omega_L) = 1$ ], Eq. (7) can then be analytically integrated and one obtains the following simple expression:

$$\bar{\sigma}(\mathbf{k}_r) = \sum_{\alpha=1}^N |f_{\alpha}|^2 + \sum_{\alpha=1}^N \sum_{\beta \neq \alpha}^N f_{\alpha} f_{\beta}^* \frac{\sin(qR_{\alpha\beta})}{qR_{\alpha\beta}}. \quad (8)$$

The second term in Eq. (7) does not vanish even after the rotational average and depends now only on the “bond lengths” ( $R_{\alpha\beta} \equiv |\mathbf{R}_\alpha - \mathbf{R}_\beta|$ ) of the molecule. This is the same expression as in UED for isotropic molecules. However, in UED experiments, only 1D angular information in  $\theta_r$  is measured. Here, for LIED, we have 2D information in both  $k_r$  and  $\theta_r$  due to the wave packet nature of the returning electrons. Translating Eq. (8) into the laboratory frame, the 2D information in  $k$  and  $\theta_k$  is obtained.

Figure 1 shows a couple of examples of the theoretical molecular interference spectra with the molecular geometry from the NIST Computational Chemistry Comparison and Benchmark Database<sup>39</sup> and the work of Gagliardi *et al.*<sup>40</sup> In detail, Figs. 1(a)–1(d) show the MIT curves in the laboratory frame at various angles between  $0^\circ$  and  $20^\circ$  for benzene ( $C_6H_6$ ), chlorobenzene ( $C_6H_5Cl$ ), *trans*-azobenzene ( $C_{12}H_{10}N_2$ ), and *cis*-azobenzene ( $C_{12}H_{10}N_2$ ). A unique feature exists in all cases: MIT curves at different laboratory angles  $\theta_k$  (defined with respect to the laser polarization) show an almost identical set of zero-crossing points (ZCPs). This feature is traced back to the fact that field-free DCs merely depend purely on the magnitude of the momentum transfer  $q$  for any combination of scattering energy and angle as one can see in Eq. (8). In a sense, these ZCPs behave like the fingerprint of molecules, uniquely determining the structures of molecules and thus giving the name, ZCP-LIED, to our new method. The clustering effect of ZCPs across various angles will be used later to guide us to extract MITs from the photoelectron momentum spectrum.

### C. Inherent limitations of the retrieval methods

One key factor in all the retrieval methods is to extract the molecular interference term from the experimental data. We discuss the limitations of all the retrieval methods and demonstrate how we deal with those limitations with our new method by reanalyzing the LIED experiments on  $O_2$  molecules with a  $2\text{-}\mu\text{m}$

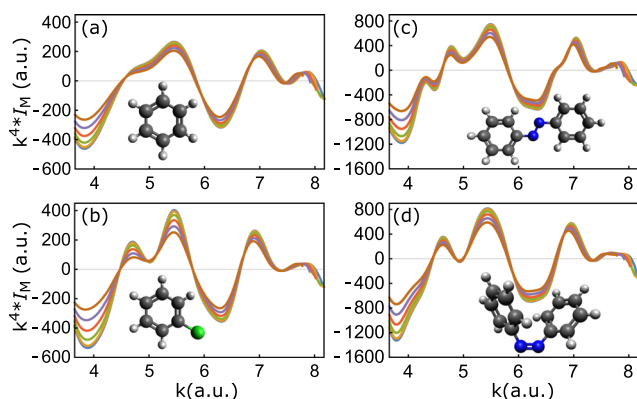


**FIG. 1.** Positions of ZCPs of the MIT curves are essentially independent of the scattering angles according to the IAM. The molecules are (a) benzene, (b) chlorobenzene, (c) *trans*-azobenzene, and (d) *cis*-azobenzene. The scattering angles are from  $0^\circ$  to  $20^\circ$  in steps of  $4^\circ$ . A larger amplitude generally corresponds to a smaller angle. The calculations are carried out with a laser intensity of  $95 \text{ TW cm}^{-2}$  and a wavelength of  $3200 \text{ nm}$ , and the MIT curves are scaled with  $k^4$  for better visualization. The molecule inside each panel is shown in the ball-and-stick model with different colors representing different atoms: dark gray (carbon), light gray (hydrogen), green (chlorine), and blue (nitrogen).

laser<sup>22</sup> at a peak intensity of  $133 \text{ TW/cm}^2$  (corresponding to a ponderomotive energy of  $U_p = 50 \text{ eV}$ ). That experiment measured the photoelectron yield as a function of momentum  $\mathbf{k}$  for a given angle at a time. The collected yield is seen in Fig. 2(a). Since the laser field is linearly polarized along the  $z$  axis, the rotation symmetry around the  $z$  axis is preserved, meaning there is no  $\phi_k$  dependence in the spectrum. That is the reason behind the choice of the transverse momentum  $k_r = (k_x^2 + k_y^2)^{1/2}$  as the vertical axis.

### 1. Selecting the applicable range of scattering data

Because of the QRS's mere validity in the high-energy part of the spectrum ( $2\text{--}10U_p$ ) and the IAM's inapplicability at low rescattering energy<sup>18</sup> ( $E_r \leq 50 \text{ eV}$ ), they together pose a limit on the lower bound of the detected momentum  $k$  to be analyzed. The range covered by the solid blue line with closed blue circles near the lower horizontal axis in Fig. 2(b) is the  $2\text{--}10U_p$  range. The range spanned by the blue solid (orange dashed, green dotted) line near the upper horizontal axis corresponds to the rescattering energy  $E_r$  between  $50$  and  $100 \text{ eV}$  for  $\theta_k = 0^\circ$ ,  $4^\circ$ , and  $20^\circ$  respectively. The larger the angle is, the smaller- $k$ -side the rescattering energy region is located at. The intersection of these two sweeps determines the minimum momentum value  $k_{\min} = 3.5 \text{ a.u.}$  for the following analysis.

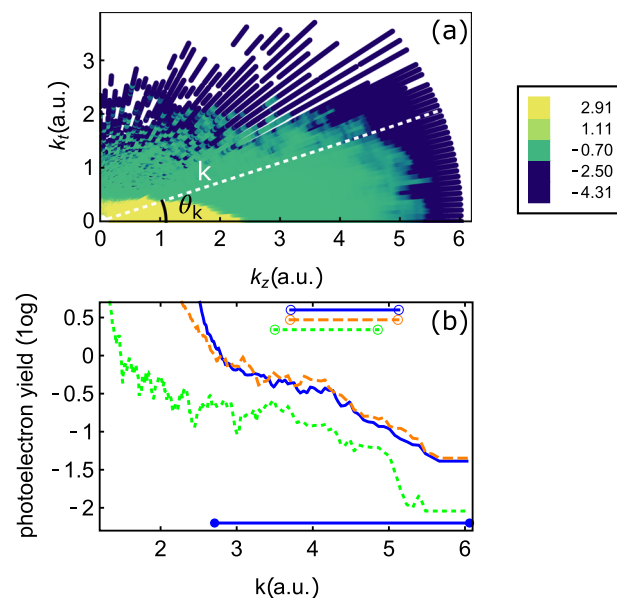


**FIG. 2.** (a) Typical two-dimensional photoelectron momentum spectrum along ( $k_z$ ) and perpendicular ( $k_r$ ) to the laser polarization. Shown are the actual experimental data taken from the work of Blaga *et al.*<sup>22</sup> for  $O_2$ -2000 nm at a laser peak intensity of  $133 \text{ TW/cm}^2$  (corresponding ponderomotive energy  $U_p = 50 \text{ eV}$ ). The yield is in logarithmic scale. (b) Illustration of the applicable momentum range of the electron spectra at various laboratory scattering angles of  $\theta_k = 0^\circ$  (blue),  $4^\circ$  (orange dashed), and  $20^\circ$  (green dotted-dashed). LIED theory utilizes the rescattered electrons, which are in the  $2U_p\text{--}10U_p$  range (covered by the solid blue circles in the  $k$  axis). IAM works for rescattering energy  $E_r$  larger than  $50 \text{ eV}$  approximately. The energy ranges of  $E_r = [50, 100] \text{ eV}$  are labeled by open blue (orange and green) circles for  $0^\circ$  ( $4^\circ$  and  $20^\circ$ ).

At the large-momentum side, data statistics plays a crucial role since the absolute DCS becomes small and very few electron counts are accumulated there. Therefore, the upper bound of the momentum  $k$  relies on a good statistics of data in this region. As one can see in Fig. 2(b), The photoelectron yield levels off at above  $k = 5.5$  a.u., which is close to  $10U_p$ , and thus, we limit the maximum momentum value to be  $k_{\max} = 5.5$  a.u.

## 2. Smoothing the DCS

With the applicable momentum range selected, we focus now only on the scattering data within that range. Taking  $0^\circ$  as an example, from the solid blue line in Fig. 2(b) [or the dotted gray line in Fig. 3(a)], we see that the measured electron yields have markedly fast oscillations, whose frequencies are too high to be corresponding to the relevant length scale of a molecule (on the order of Å). Therefore, to remove those incidental fluctuations, we first apply a Gaussian filter to smooth out the laboratory-frame DCS. The range of momentum  $k$  is chosen to be  $\{3.5, 5.5\}$  a.u. A Gaussian filter convolves the input data array (assume  $\{a_1, a_2, \dots, a_M\}$ ) with a Gaussian kernel ( $G_{ij}$ ) of dimensions  $(2N+1) \times (2N+1)$ . To put it in a simple way, a Gaussian filter replaces each data point by a

linear combination of its  $2N$  nearest neighbors with weights specified by a Gaussian kernel. Specifically, the smoothed list (assume  $\{\tilde{a}_1, \tilde{a}_2, \dots, \tilde{a}_M\}$ ) is written in terms of the input data as

$$\tilde{a}_k = \sum_{i=1}^{2N+1} \sum_{j=1}^{2N+1} G_{ij} a_{k-(N-j+1)} \quad (9)$$

for  $k = 1, 2, \dots, M$ . The flat padding is imposed, which means  $a_i = a_1$  for  $i < 1$  and  $a_i = a_N$  for  $i > N$ . Due to the choice of padding, the smoothed data at boundaries should be used carefully. The degree of smoothness is determined by the number of neighbors included. The larger  $N$  is, the greater the degree of smoothness is. From now on, we would refer to the parameter  $N$  as the Gaussian smoothness factor (GSF). The smoothed curve with GSF = 160 (or a radius of  $160 \times 0.00603 = 0.965$  a.u. in the  $O_2$ -2000 nm example where the step size of  $k$  is 0.00603 a.u.) is shown as the solid blue line in Fig. 3(a).

## 3. Extracting MIT and ZCPs

After smoothing, we apply a polynomial fit ( $\sum_{i=0}^n c_i k^i$ ) to the smoothed data to find the background curve or the empirical atomic term. The coefficients  $c_i$  are determined by the standard least squares fitting. From scattering theory, we learn that the field-free electron-atom DCS at high energy is a strictly decreasing function of energy for fixed scattering angles. Transformation to the laboratory frame does not change this feature. Therefore, the order of the polynomial should not be too high to avoid over fitting. Choices of  $n = 2-4$  are often used in the literature and the examples shown in the current paper. In Fig. 3(b), because of the small range in  $k$ , we choose a quadratic polynomial fitting to get the background curve [see the black dashed line in Fig. 3(b)].

Next, subtracting the fitted background from the smoothed laboratory-frame DCS, we get the laboratory-frame MIT  $I_M$  in Fig. 3(c). Repeating the procedure for other angles, the 2D laboratory-frame MIT distribution  $I_M$  as a function of  $\{k, \theta_k\}$  is extracted and shown in Fig. 3(f). Six angles from  $\theta_k = 0^\circ$  to  $5^\circ$  in steps of  $1^\circ$  are used. We use the same red color for these six different angles since the order is not important and one does not need to make distinction between them.

In the process of extracting the 2D MIT in the laboratory frame, there are multiple “numerical” parameters to be tuned: (i) the range of momentum  $k$  for retrieval, (ii) the degree of smoothness, or GSF, and (iii) the order and coefficients of the polynomial function. The tuning process of these parameters is an optimization process of finding the best point in this multidimensional parameter space formed by (i)–(iii) to ensure that MITs at different angles all give similar sets of ZCPs, which is a general feature predicted by the IAM.

The ZCP distribution is intrinsic to the molecular structures. Nevertheless, the background subtraction affects the ZCP positions in a practical way. Thus, a stability test of the ZCPs is needed. Based on our analysis, the ZCPs close to the end of the chosen region are affected more by the polynomial fitting than those in the center. As a result, in Figs. 3(d) and 3(e), we test the robustness of the ZCP against the choice of  $k_{\min}$  and  $k_{\max}$ , which define the momentum range. By varying  $k_{\min}$  in  $[3.43, 3.67]$  a.u. [from brighter blue to darker blue in Fig. 3(d)] for a fixed final momentum, we observe that the first ZCP varies its position in the same order of magnitude as the change in  $k_{\min}$ . It shows that the first ZCP near 3.7 a.u. is not stable. Similarly, we vary  $k_{\max}$  in  $[5.49, 5.79]$  a.u. [from darker orange to

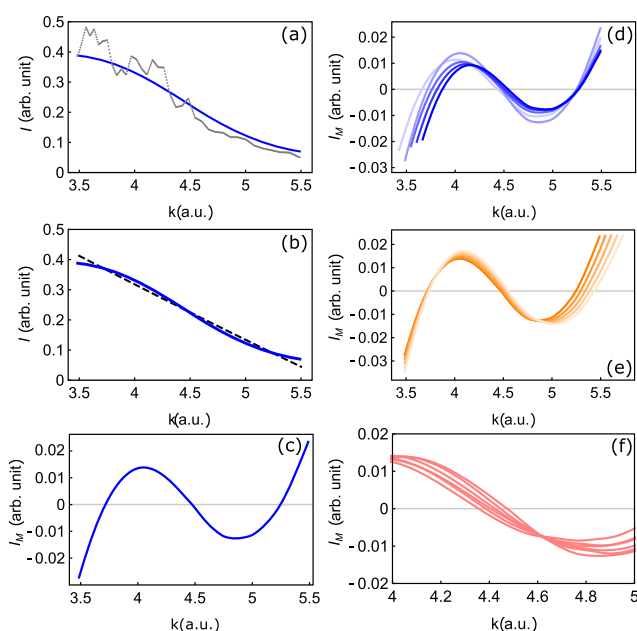


**FIG. 3.** Illustration of steps in extracting the MIT curves.  $0^\circ$  is used in (a)–(e). (a) The experimental DCS (gray dotted) is processed with a Gaussian filter to obtain a smoothed curve shown in blue. GSF = 160 (or a radius of 0.96 a.u.) is used. (b) Fit the smoothed curve (blue) with a quadratic polynomial (black dashed line) to get the background. (c) Subtract the two curves in (b) to obtain the MIT curve. Note that the fitted MIT curves depend on the range of  $k$  used in the fitting. In (d) and (e), we show how the MIT curve is varied when the initial momentum point (d) or the end point (e) is varied. These together show that the ZCP in the middle is not sensitive to the choice of the end points, but the ZCPs close to the two ends vary wildly. To use MIT in our analysis, we exclude the momentum range containing the two outermost ZCPs. In (f), we show that the MIT to be analyzed is in  $[4.0, 5.0]$  a.u. The same procedure is used to obtain MIT curves for other five angles ( $1^\circ$ – $5^\circ$  in steps of  $1^\circ$ ). These curves, which are extracted from Fig. 2, will be used to extract the bond length of  $O_2$ .

lighter orange in Fig. 3(e)] for a fixed  $k_{\min}$ . We see that the third ZCP near 5.3 a.u. is again not stable. We thus conclude that only the middle ZCP is robust against the choice of momentum range and thus is used in the retrieval to determine the molecular structure. Limited by the inverse quadratic scaling law of the cutoff energy in wavelength, only one ZCP for each angle is managed to be extracted in the O<sub>2</sub>-2000 nm case. Even so, it does not prevent us from using the ZCP-LIED method since the molecular oxygen is a simple molecule with only a single bond length. For more complicated molecules, we need more ZCPs to determine structures.

Once the 2D ZCP distribution is found, we then feed it to the genetic algorithm (GA)<sup>41,42</sup> for structural retrieval. The fitness function  $f_{\text{ZCP}}(\vec{X})$  is defined by the negative value of the sum of the squares of the difference between the set of ZCPs of the experimental data and the one determined by a trial set of the structural parameters,

$$f_{\text{ZCP}}(\vec{X}) = -\sum_{a=1}^{N_a} \sum_{i=1}^{N_r} (\text{ZCP}_{a,i}^{\text{exp}} - \text{ZCP}(\vec{X})_{a,i}^{\text{theory}})^2, \quad (10)$$

where  $\vec{X}$  denotes the structural parameters (bond lengths and angles),  $a$  labels the discretized angle, and  $i$  labels the  $i$ th ZCP of the corresponding angle from  $i = 1$  to  $N_r$ .  $N_a$  is the total number of the angles used, and  $N_r$  is the number of roots for each individual angle. Unless symmetry is imposed, in the most general case, we would need  $C_2^N$  structural parameters for a given molecule with  $N$  atoms. The actual step in the angle would be determined by the experiments, and the available number of ZCPs is determined by the measured momentum range and the stability analysis. Using two-dimensional information for retrieval effectively increases the usable momentum range in the photoelectron momentum spectrum, which mitigates the finite momentum-range problem and the decrease in the usable momentum for retrieval from the stability analysis of ZCP. Beyond that, 2D fitting also minimizes the potential bias from using only one angle.

Apart from the fitness function defined in Eq. (10), we analyze the extracted 2D MIT distribution using the conventional fitness function (the sum of the squares of the difference between the experimental data and the theory one determined by the structure  $\vec{X}$ ) as well, which is

$$f_{\text{SD}}(\vec{X}) = -\sum_{a=1}^{N_a} \sum_{i=1}^{N_k} (I_M^{\text{exp}}_{a,i} - c \times I_M(\vec{X})_{a,i}^{\text{theory}})^2, \quad (11)$$

where  $a$  and  $i$  label the discretized angle and momentum.  $N_a$  is again the total number of discrete angles, and  $N_k$  is the number of discrete momentum points for a given angle labeled by the index  $a$ . The sizes of  $N_a$  and  $N_k$  are determined by the experimental data. Although Eq. (11) uses the conventional least squares approach, to emphasize the 2D nature, we refer to this method as the 2D-MIT method. Note that we have used an overall scaling factor  $c$  to bring the theoretical MITs to the scale of the experimental MITs.

Both the ZCP and the 2D-MIT methods would be used for our analysis as a consistency check of the retrieved results. Even so, we comment that fitting ZCPs is generally more advantageous than MITs because the ZCP method is insensitive to the oscillation amplitudes of the MITs, meaning it treats every part of MITs on an equal footing instead of favoring the large amplitude parts as in the

second fitness function of Eq. (11). This avoids putting an incorrectly significant weight on the large amplitude part of MITs from possibly skewed ratios of the oscillation amplitudes between different peaks/valleys during the data-taking or extraction process. An additional benefit is that we have one less fitting parameter (i.e., the overall normalization factor  $c$ ), which speeds up the optimization process.

It is worth mentioning that using ZCPs for retrieval has also been explored in the UED community<sup>43</sup> (see the second method of background subtraction in Sec. II D, called the UED-2 method here). However, they have used the ZCPs to determine the background curve, which passes through those critical points giving a zero value in the molecular term after subtracting the background from the DCS. They have adopted a “simultaneous” optimization to determine the background curve as well as the optimal theoretical fit with a standard fitness function measuring the difference between the theoretical and experimental data. To test the effect of different background subtraction methods, we have applied the UED-2 method in OCS molecules for five different angles separately and find that the background curves still vary (IAM theory predicts the same background for all angles) and give a ZCP distribution of a width around 0.3 a.u. as in Fig. 4 even though the extracted molecular terms match very well (almost on top of each other) with the reconstructed ones. Therefore, we find that the same problem we encounter in LIED also exists in UED. We are convinced that a consistency check across different retrieval methods is key in successful molecular structural retrieval and using the 2D feature of the LIED data provides us a way to reach a reliable answer.

#### D. Re-evaluation of O<sub>2</sub> bond length using the two-dimensional retrieval method

Figures 5(a) and 5(b) show the retrieval results using  $f_{\text{SD}}$  and  $f_{\text{ZCP}}$  as fitness functions with the simplest isotropic IAM. Comparisons of the experimental MITs (red solid line) and the reconstructed theoretical MITs [gray dashed line in Fig. 5(a) and gray dotted line in Fig. 5(b)] are shown. Note that there are six reconstructed MIT curves in each panel, overlapping with each other, with a one-to-one

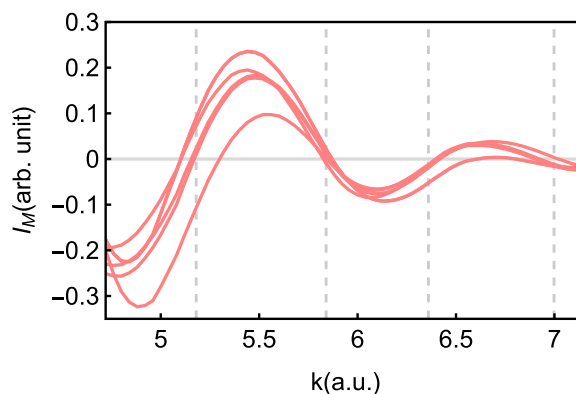
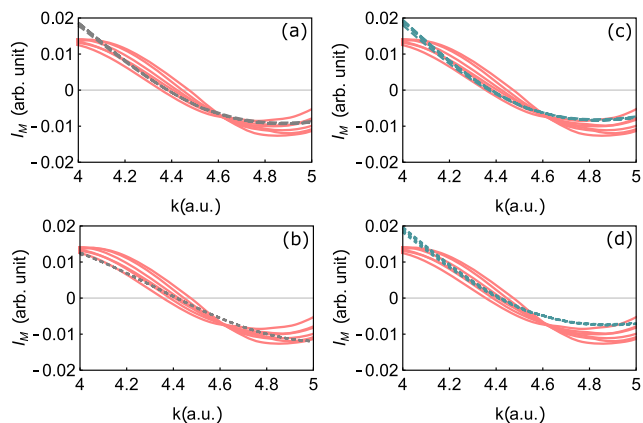


FIG. 4. Extracted MIT curves (solid lines) for OCS molecules at five different angles using the UED-2 method.<sup>43</sup> The vertical dashed lines are the mean ZCP positions with our polynomial fitting.



**FIG. 5.** Retrieval of  $O_2$ -2000 nm. [(a) and (b)] The simplest isotropic IAM is used. We see that the 2D-MIT [(a), gray dashed line] and the ZCP-LIED [(b), gray dotted line] methods show little differences. In (c) and (d), the molecules are treated by including the angle-dependent ionization rate with the 2D-MIT [(c), green dashed line] and the ZCP [(d), green dotted line] methods. The set of red solid curves is the extracted MIT curves as in Fig. 3(f).

correspondence to the experimental ones. It is the clustering of the MIT curves  $I_M$  among different angles that we expect from IAM, so we do not make efforts to label out different angles with different colors or styles. The retrieved bond lengths are  $R_{OO} = 1.09$  and  $1.08$  Å, respectively, demonstrating that these two different fitness functions are consistent within  $0.01$  Å. In particular, we want to emphasize that the reconstructed curves in Fig. 5(b) pass through approximately the mean value of the six ZCP positions despite that we fit the locations of the ZCPs only, regardless of the amplitude of MIT curves.

In Figs. 5(c) and 5(d), we study the orientation-dependent tunneling-ionization-rate effect on the retrieved bond length with our 2D-MIT [Fig. 5(c)] and ZCP-LIED [Fig. 5(d)] methods. The retrieved bond lengths are  $R_{OO} = 1.16$  and  $1.15$  Å, respectively. For reference, the bond length for neutral  $O_2$  molecules in the ground state is  $1.21$  Å.<sup>44</sup> As in the case of isotropic ionization, it shows that our two methods give consistent retrieved bond lengths.

Since the bond length can be retrieved from each fixed scattering angle also, it is pertinent to provide the “error” for the retrieved bond length. Using ZCP-LIED, we extract the bond length to be  $1.08^{+0.02}_{-0.01}$  or  $1.15^{+0.02}_{-0.01}$  Å when ionization is not included or included. Rigorously speaking, in LIED, ionization rates should be included in the retrieval. From another perspective, for nonlinear molecules, the inclusion of the ionization rate as in Eq. (7) would require knowledge of ionization rates and a three-dimensional integration over the alignment distributions. For  $O_2$  and  $N_2$ , we present results including ionization rates to calibrate the typical errors of the retrieved results. The comparison would offer an estimate of the error for using the simplified model.

### III. REANALYSIS OF PREVIOUS EXPERIMENTAL DATA

To demonstrate our method, we test it on the following molecules:  $O_2$ ,  $N_2$ ,  $CO_2$ ,  $OCS$ , and  $H_2O$ . The data for  $O_2$  and  $N_2$  are from the work of Blaga *et al.*<sup>22</sup> The data for  $OCS$  are from the

work of Sanchez *et al.*<sup>28</sup> The data for  $H_2O$  are from the work of Liu *et al.*<sup>26</sup>

#### A. Molecular oxygen at different wavelengths

SD-LIED has been applied to oxygen molecules to determine its structure under strong fields at three different mid-infrared wavelengths ( $1.7$ ,  $2.0$ , and  $2.3$  μm).<sup>22</sup> We reexamine the same experiment with our new two-dimensional analysis.

The left column of Fig. 6 shows comparisons of the extracted MIT curves  $I_M$  with the reconstructed ones with the isotropic IAM in (a) and the ionization-weighted isotropic IAM in (b) using the 2D-MIT method for a wavelength of  $1700$  nm. The right column of Fig. 6 shows the equivalent figures for a wavelength of  $2300$  nm. Due to the quadratic scaling law with wavelength, the available momentum range for  $1700$  nm is the narrowest among the three. The same data are analyzed with the ZCP method as a consistency check in Fig. 7.

Putting Figs. 5 and 6 together, we see that the extracted experimental ZCPs shift to the higher-momentum side as the wavelength increases. We summarize the retrieved bond lengths from Figs. 5–7 in Table I including the ones from the original analysis.<sup>22</sup> Our results using two different approaches agree well with each other within an accuracy of  $0.01$  Å in all three wavelengths and have about a  $0.05$  Å difference from the ones in the work of Blaga *et al.*<sup>22</sup> except the  $2.3$ -μm case. It could be due to a larger error in the experimental data as one can see from the larger variations between different angles in the set of the  $2300$  nm data [red solid curves in Fig. 6(c)]. Furthermore, from our analysis of all three wavelengths, we conclude that the ionization rate could cause a difference in the bond length up to  $0.1$  Å.

We comment that the highest occupied molecular orbital (HOMO) of oxygen is an antibonding orbital, and thus, the removal of one electron would cause the bond length to shrink. For longer wavelengths, the return time is longer, and thus, the bond length would shrink more. Our retrieved data from different methods

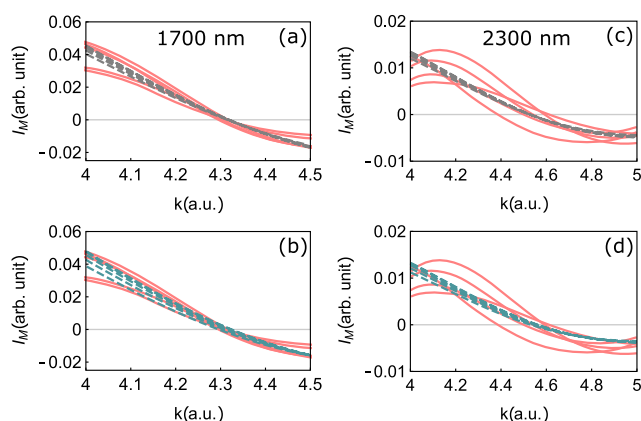


**FIG. 6.** Retrieval using the 2D-MIT method. [(a) and (b)] For  $O_2$ - $1700$  nm with the inclusion of isotropic (gray dashed) and angle-dependent (green dashed) ionization rate. The corresponding retrieved bond lengths are  $1.09$  and  $1.17$  Å. [(c) and (d)] For  $O_2$ - $2300$  nm with retrieved bond lengths of  $1.06$  and  $1.12$  Å.

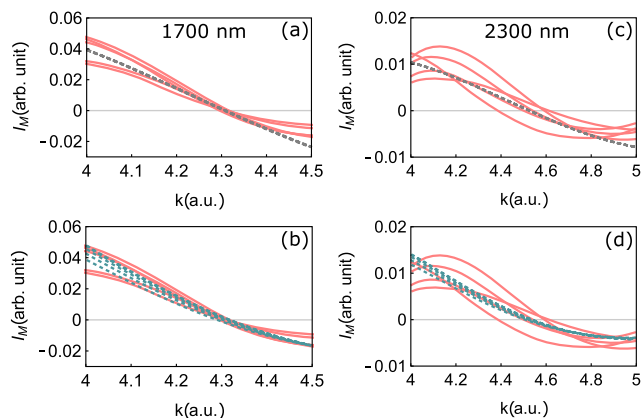


**FIG. 7.** Similar to Fig. 6, but with the ZCP-LIED method, we compare retrieved results with the isotropic [(a) and (c); gray dotted] or the angle-dependent [(b) and (d); green dotted] ionization rates for  $O_2$ -1700 nm [(a) and (b)] and  $O_2$ -2300 nm [(c) and (d)]. The retrieved bond lengths are (a) 1.09, (b) 1.16, (c) 1.07, and (d) 1.13 Å.

shown in Table I are consistent with this prediction, while the ones in the work of Blaga *et al.*<sup>22</sup> did not.

## B. Molecular nitrogen at different wavelengths

Similar to  $O_2$  molecules, we reexamine the experiments on  $N_2$  molecules at the same wavelengths.<sup>22</sup> The left (middle, right) column of Fig. 8 shows comparisons of the extracted MIT curves  $I_M$  with the reconstructed ones with the isotropic IAM in panel (a) [(c) and (e)] and the ionization-weighted IAM in panel (b) [(d) and (f)] using the 2D-MIT method for a wavelength of 1700 nm (2000, 2300 nm). For 2000 and 2300 nm, we are able to extract two ZCPs for each angle with a wider momentum range compared to 1700 nm.

We summarize the retrieved bond lengths of  $N_2$  molecules in Table II including the ones from the original analysis.<sup>22</sup> For comparison, the bond length of the ground state  $N_2$  molecules is 1.10 Å.<sup>44</sup> For the ZCP method, we also calculate the estimated error of the retrieved bond length. From the retrieved bond lengths, we see that (1) the 2D-MIT and ZCP methods are consistent within the accuracy of 0.02 Å and (2) the effect of ionization rate is less significant for  $N_2$  compared to  $O_2$  molecules and acts in the opposite direction. The difference in bond length caused by ionization for all three wavelengths of  $N_2$  is all under 0.05 Å.

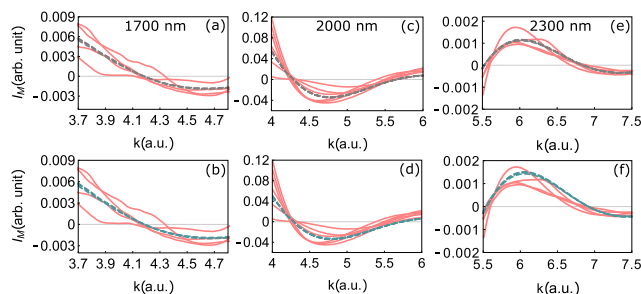


**FIG. 8.** Retrieval using the 2D-MIT method. [(a) and (b)] For  $N_2$ -1700 nm with the isotropic (gray dashed line) and angle-dependent (green dashed line) ionization rates. The corresponding retrieved bond lengths are 1.14 and 1.10 Å. [(c) and (d)] For  $N_2$ -2000 nm with retrieved bond lengths of 1.13 and 1.10 Å. [(e) and (f)] For  $N_2$ -2300 nm with retrieved bond lengths of 1.17 and 1.14 Å.

Comparing our results with the work of Blaga *et al.*,<sup>22</sup> the differences between them are all within 0.05 Å. We point out that the bond lengths as a function of wavelength change in the opposite direction in ours and Blaga *et al.*<sup>22</sup> Since the HOMO of nitrogen is a bonding orbital, the removal of an electron would cause the bond length to expand. Thus, the bond length should increase with the wavelength of the laser used [also as suggested by the theoretical calculations in Fig. 2(e) of the work of Blaga *et al.*<sup>22</sup>]. Our ZCP-LIED method correctly reflects the trend from theory, while Blaga *et al.*<sup>22</sup> ran in a completely opposite direction. The right trend from our ZCP method (other than the 2D-MIT method) hints that the ZCP method generally works better than the 2D-MIT one.

For the rest of the examples, we would only present the results using the ZCP-LIED method for the reason of conciseness and the advantages we have seen even though we have used both methods for all the molecules. As in the cases of  $N_2$  and  $O_2$  molecules, both methods give consistent results.

## C. Carbon dioxide molecules

The photoelectron momentum distribution of  $CO_2$  molecules exposed in a linearly polarized laser at 2  $\mu\text{m}$  is recorded. The peak intensity is 170  $\text{TW}/\text{cm}^2$ , leading to a ponderomotive energy of  $U_p = 63$  eV. Unlike  $O_2$  and  $N_2$ , this LIED experiment on  $CO_2$  molecules has never been reported before.

We analyze the photoelectron spectrum of  $CO_2$  by first extracting the molecular interference terms  $I_M$  at angles between  $0^\circ$  and

**TABLE I.** Summary of the retrieved bond lengths of oxygen molecules from our 2D-MIT and ZCP methods and the work of Blaga *et al.*<sup>22</sup> in units of Å for three wavelengths.

Wavelength (nm)	2D-MIT	ZCP	Blaga <i>et al.</i>	2D MIT	ZCP
	Isotropic				
1700	1.09	1.09 <sup>+0.01</sup> <sub>-0.00</sub>	1.10	1.17	1.16 <sup>+0.01</sup> <sub>-0.00</sub>
2000	1.09	1.08 <sup>+0.02</sup> <sub>-0.01</sub>	1.11	1.16	1.15 <sup>+0.02</sup> <sub>-0.01</sub>
2300	1.06	1.07 <sup>+0.03</sup> <sub>-0.02</sub>	1.02	1.12	1.13 <sup>+0.04</sup> <sub>-0.02</sub>

**TABLE II.** Summary of the retrieved bond lengths for nitrogen molecules from our methods and the work of Blaga *et al.*<sup>22</sup> in units of Å for three wavelengths.

Wavelength (nm)	2D MIT	ZCP	Blaga <i>et al.</i>	2D MIT	ZCP
	Isotropic		With the MO-ADK rate		
1700	1.14	1.14 <sup>+0.02</sup> <sub>-0.04</sub>	1.15	1.10	1.10 <sup>+0.02</sup> <sub>-0.04</sub>
2000	1.13	1.15 <sup>+0.03</sup> <sub>-0.02</sub>	1.14	1.10	1.12 <sup>+0.02</sup> <sub>-0.02</sub>
2300	1.17	1.17 <sup>+0.00</sup> <sub>-0.01</sub>	1.12	1.14	1.15 <sup>+0.00</sup> <sub>-0.01</sub>

5° in steps of 1°. The 2D distribution of the molecular interference term is then used to retrieve the bond length with the isotropic IAM. We find three solutions that are comparably close to the extracted  $I_M$  in the parameter space formed by the bond length of  $R_{CO}$  and the bond angle of  $\theta_{OCO}$ . These three solutions are (i)  $R_{CO} = 1.10$  Å and  $\theta_{OCO} = 90^\circ$ , (ii)  $R_{CO} = 1.04$  Å and  $\theta_{OCO} = 113^\circ$ , and (iii)  $R_{CO} = 1.05$  Å and  $\theta_{OCO} = 180^\circ$ . The three corresponding reconstructed MIT sets are shown in Figs. 9(a)–9(c). The three collected reconstructed curves reproduce the experimental one to a fair degree. With the variance in the MIT curves among different angles, it is not clear which solution is the optimal one. To resolve this issue, we calculate the error map using the absolute value of Eq. (10) shown in Fig. 9(d). We eliminate the results in the gray shaded region, in which the structural parameters either give only one ZCP or inverted MIT curves with peaks on the side of  $I_M > 0$ . Three minima, which are close in magnitude, are evidently recognized and correspond to the three solutions in (i)–(iii). The three solutions all give a similar bond length around 1.05 Å but drastically different bond angles. From the landscape of the error map, we conjecture that the solution with a bond angle of 180° might be the best one given that the valley there is wider and shows a more gradual descent to the bottom.

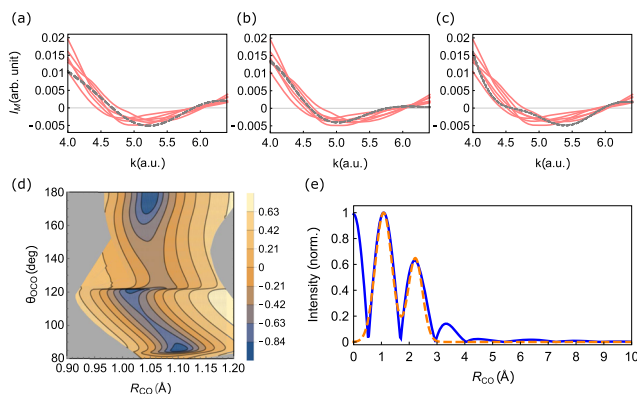


**FIG. 9.** Comparisons of the extracted MIT curves for  $\text{CO}_2$  molecules (solid red line) and the ZCP-LIED reconstructed ones (gray). GSF = 180 (or a radius of 1.23 a.u.) is used. These three solutions give a similar bond length around 1.05 Å, but quite different bond angles, which are 90° in (a), 113° in (b), and 180° in (c). (d) The error map in the parameter space formed by  $R_{CO}$ , bond length, and  $\theta_{OCO}$ . The error is calculated based on the ZCP fitness function in Eq. (10). Three minima are found to be close to each other. (e) The normalized intensity of Fourier-transforming the interference signal at  $\theta_k = 0^\circ$  is shown in solid blue. The dashed orange curve shows the double-Gaussian fit to the normalized intensity. The values are peaked at 1.08 and 2.22 Å, which correspond to  $R_{CO}$  and  $R_{OO}$ .

To confirm that, we perform the Fourier analysis. Fourier cosine transforming the molecular interference term, we arrive at a radial distribution with two dominant peaks centered at 1.08 and 2.22 Å. They result in a bond angle of 180°. With this linear-geometry solution [solution (iii)], we estimate the error to be  $R_{CO} = 1.05^{+0.02}_{-0.02}$  Å and  $\theta_{OCO} = 180^{+0}_{-14}$ °. For reference, we include the ground state geometry of  $\text{CO}_2$  here:  $R_{CO} = 1.16$  Å and  $\theta_{OCO} = 180^\circ$ .<sup>45</sup> The example of  $\text{CO}_2$  demonstrates how different methods could potentially complement each other and give a well-grounded solution. A similar philosophy has also been adopted in the retrieval of  $\text{C}_{60}$  molecules.<sup>46</sup>

#### D. Carbonyl sulfide molecules

The final two examples—OCS (this subsection) and  $\text{H}_2\text{O}$  (in Subsection III E)—are experiments done at ICFO.<sup>26</sup> Using a reaction microscope,<sup>47</sup> they measure electrons in coincidence with molecular ions in 3D detection. The wavelength used is 3200 nm, which leads to a large ponderomotive energy. In the OCS case, the laser peak intensity is  $9.5 \times 10^{13}$  W/cm<sup>2</sup>, so  $U_p$  is 90 eV. This large value of  $U_p$  leads to electron energies all the way to  $10U_p = 900$  eV (or  $k = 8.1$  a.u.). The wide momentum range allows us to extract a 2D molecular interference distribution with four ZCPs for every scattering angle.

Figure 10(a) shows the collected molecular interference terms  $I_M$  for 33 scattering angles  $\theta_k$  in  $[0.0, 8.0]^\circ$  in steps of  $\Delta\theta_k = 0.25^\circ$  across the momentum range of [4.72, 7.16] a.u. in the laboratory frame. The amplitude of the molecular interference terms decreases as the momentum increases because of a reduced scattering probability with an increasing electron momentum. Figure 10(b) provides an alternative view of the 2D molecular interference terms  $I_M$ . Instead of showing the real value of  $I_M$ , we represent the positive (negative) values of  $I_M$  as magenta (cyan) dots. The sign-changing boundaries are the locations of the ZCPs. Figure 10(c) shows the ZCP distributions for each of the four ZCPs. To better visualize the variance of the distribution, we subtract the mean of the ZCP positions, so it becomes the origin of the momentum axis. One limitation of using a long wavelength is that the signal-to-noise ratio at large momenta becomes relatively low. This is reflected by the fact that the fourth ZCP distribution located at the highest momenta has the largest variance compared to the other three.

Since there are multiple ZCPs and more angles in the OCS example, we determine the error bars by retrieving the 2D set of data shifted by the average bandwidth of the four ZCP distributions instead of retrieving the individual angle. The optimal bond lengths found using the ZCP-LIED method are  $R_{CO} = 1.19^{+0.01}_{-0.01}$  Å,

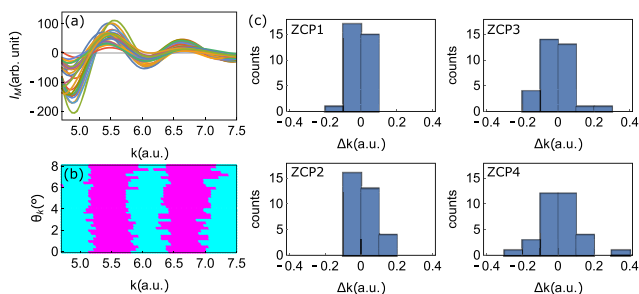


**FIG. 10.** (a) Extracted MIT curves as a function of the detected momentum  $k$  at 33 different angles  $\theta_k$  between  $0^\circ$  and  $8^\circ$  for OCS molecules. GSF = 12 (or a radius of 0.48 a.u.) is used. Different colors mean different angles. (b) Alternative view of the extracted MIT data. The magenta (cyan) color means the MIT is positive (negative). The sign-changing positions are the ZCPs. Four zero-crossing points are seen in total. (c) Distribution of the four ZCPs with respect to the average ZCP positions ( $\Delta k = k_{ZCP} - \langle k_{ZCP} \rangle$ ). The roots 1–4 are arranged in ascending order of momentum. The last ZCP has the widest distribution due to the weakest signal-to-noise ratio.

$R_{CS} = 1.72^{+0.02}_{-0.02}$  Å, and  $R_{OS} = 2.72^{+0.02}_{-0.02}$  Å. From that, we calculate the bond angle to be  $138^{+30}_{-3}$ , showing that the OCS molecules become bent and asymmetrically stretched after being exposed to the strong field. This result is consistent with the FT-LIED method,<sup>28</sup> where they have  $R_{CO} = 1.06$  Å,  $R_{CS} = 1.87$  Å, and  $R_{OS} = 2.78$  Å (giving  $\theta_{OCS} = 142^\circ$ ), and is also confirmed by the quantum–classical calculations.<sup>28</sup> For reference, the ground state geometry of the OCS molecules is  $R_{CO} = 1.16$  Å,  $R_{CS} = 1.56$  Å, and  $R_{OS} = 2.72$  Å (i.e., a linear molecule with  $\theta_{OCS} = 180^\circ$ ).<sup>45,48</sup>

We would like to comment that the structure of OCS has also been examined by Karamatskos *et al.*<sup>34</sup> recently. They have found that the OCS molecules stay basically unchanged in the laser field and remain linear. We attribute the difference to the laser properties, in which a shorter wavelength of 2- $\mu$ m laser was used.

### E. Water molecules

A 3.2- $\mu$ m linearly polarized laser with a peak laser intensity of  $1.6 \times 10^{14}$  W/cm<sup>2</sup> was used in imaging the water molecules.<sup>26</sup> The corresponding ponderomotive energy is 150 eV, which is the largest one among all the cases examined in this work. This large value of  $U_p$  leads to a wide range of momentum available for our analysis.

Figure 11(a) shows the collected molecular interference terms  $I_M$  for 11 scattering angles  $\theta_k$  in  $[0.0, 10.0]^\circ$  in steps of  $\Delta\theta_k = 1^\circ$  across the momentum range of  $[5.0, 10.7]$  a.u. in the laboratory frame. The signal at high momenta larger than 8 a.u. has a very low contrast. To better visualize  $I_M$ , we rescale the data for  $k \geq 8$  by the factor  $3^{k-8}$  in Fig. 11(b). Similar to Figs. 10(b) and 10(c), we use the sign of  $I_M$  to present the 2D molecular interference distribution in Fig. 11(c) and show the ZCP distributions for the first four ZCPs, respectively, in Fig. 11(d). The ZCP distribution has a larger deviation from its mean located at the larger momentum.

As in the OCS case, Using the ZCP-LIED method, we have retrieved the bond lengths with the isotropic IAM to be  $R_{OH} = 1.17^{+0.02}_{-0.02}$  Å and  $R_{HH} = 1.86^{+0.06}_{-0.06}$  Å. The calculated HOH bond angle is  $105^{+50}_{-5}$ . Comparing with the results from the FT-LIED method,<sup>26</sup>

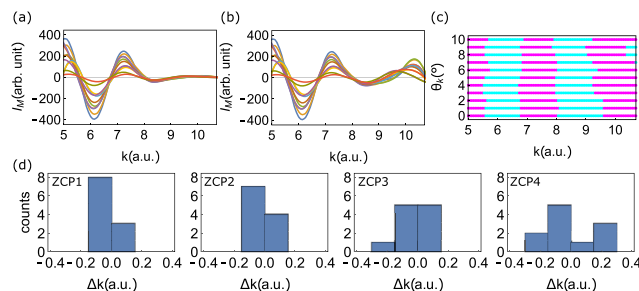


**FIG. 11.** (a) Extracted MIT curves of H<sub>2</sub>O molecules as a function of the detected momentum  $k$  at 11 different angles between  $0^\circ$  and  $10^\circ$ . GSF = 18 (or a radius of 1.08 a.u.) is used. Different colors mean different angles. (b) The amplitude of MIT at large momentum  $k$  is extremely small. To better visualize the curves, in particular, the ZCPs, we scale the MIT by the factor of  $3^{k-8}$  for  $k \geq 8$ . (c) Alternative view of the extracted MIT data. The magenta (cyan) color means the MIT is positive (negative). The sign-changing positions are the ZCPs. Four ZCPs are seen in total. (d) Distribution of the four ZCPs with respect to the average ZCP positions ( $\Delta k = k_{ZCP} - \langle k_{ZCP} \rangle$ ). The roots 1–4 are arranged in ascending order of momentum.

$R_{OH} = 1.242$  Å and  $R_{HH} = 2.037$  Å, resulting in a  $110^\circ$  bond angle. For reference, the ground state geometry of the water molecules is  $R_{OH} = 0.96$  Å and  $R_{HH} = 1.52$  Å with a bond angle of  $104.5^\circ$ .<sup>49</sup>

### IV. CONCLUSIONS

We propose a novel retrieval method based on LIED by directly analyzing the full two-dimensional laboratory-measured photoelectron spectra. Two different 2D approaches are provided for analysis and are used as a consistency check to combat the practical finite momentum-range problem, where bond lengths are to be retrieved in every iterative fitting method. We have benchmarked our method with a number of examples whose results are consistent with the existing methods, but with the additional possibility to provide estimates of errors that depend on the retrieval methods. These errors are on top of the standard statistical experimental errors, which are not addressed here.

In addition, we have demonstrated that the tunneling ionization has an effect of around 0.1 Å on the bond lengths. Within this accuracy, we have shown that using the simplest model, the isotropic IAM, can already give decent estimations of the molecular structures. It shows promises of applying the simplest IAM to somewhat large molecular systems, in which the tunneling ionization rates are difficult to find.

With a larger molecular size, the number of unknown bond lengths increases. This makes any iterative fitting method harder to converge. While our 2D method alleviates the problem by extending the usable momentum space, a larger molecular system would demand a wider range of experimental data in the momentum space, which may not be practical. No matter how accurately the molecular interference terms have been reproduced, the dependence of the retrieved bond lengths on the momentum range of the experimental data continues to pose challenges. For the present, we raise awareness that structure retrieval based on electron diffraction data has some limitations when applied to large molecules.

## ACKNOWLEDGMENTS

S.-J.W., J.D., and C.D.L. were supported by Chemical Sciences, Geosciences, and Biosciences Division, Office of Basic Energy Sciences, Office of Science, U.S. Department of Energy, under Grant No. DE-FG02-86ER13491. C.I.B. acknowledges James R. Macdonald Laboratory, supported by the U.S. Department of Energy (DOE), Office of Basic Energy Sciences, Chemical Sciences, Geosciences, and Biosciences Division (Grant No. DE-FG02-86ER13491). L.F.D. acknowledges financial support from the U.S. Department of Energy under Grant No. DE-FG02-04ER15614. J.B. acknowledges financial support from the European Research Council for ERC Advanced Grant “TRANSFORMER” (Grant No. 788218), the ERC Proof of Concept Grant “miniX” (Grant No. 840010), FET-OPEN “PETACom” (Grant No. 829153), FET-OPEN “OPTologic” (Grant No. 899794), Laserlab-Europe (Grant No. EU-H2020 654148), MINECO for Plan Nacional FIS2017-89536-P, AGAUR for 2017 SGR 1639, MINECO for “Severo Ochoa” (Grant No. SEV-2015-0522), Polish National Science Center Symfonia (Grant No. 2016/20/W/ST4/00314), Fundacio Cellex Barcelona, the CERCA Programme/Generalitat de Catalunya, and the Alexander von Humboldt Foundation for the Friedrich Wilhelm Bessel Prize.

## AUTHOR DECLARATIONS

## Conflict of Interest

The authors have no conflicts to disclose.

## DATA AVAILABILITY

The data that support the findings of this study are available from the corresponding author upon reasonable request.

## REFERENCES

- <sup>1</sup>R. Neutze, R. Wouts, D. van der Spoel, E. Weckert, and J. Hajdu, “Potential for biomolecular imaging with femtosecond X-ray pulses,” *Nature* **406**, 752–757 (2000).
- <sup>2</sup>J. Küpper, S. Stern, L. Holmegaard, F. Filsinger, A. Rouzée, A. Rudenko, P. Johnson, A. V. Martin, M. Adolph, A. Aquila, S. Bajt, A. Barty, C. Bostedt, J. Bozek, C. Caleman, R. Coffee, N. Coppola, T. Delmas, S. Epp, B. Erk, L. Foucar, T. Gorkhover, L. Gumprecht, A. Hartmann, R. Hartmann, G. Hauser, P. Holl, A. Hömke, N. Kimmel, F. Krasniqi, K.-U. Kühnel, J. Maurer, M. Messerschmidt, R. Moshhammer, C. Reich, B. Rudek, R. Santra, I. Schlichting, C. Schmidt, S. Schorb, J. Schulz, H. Soltau, J. C. H. Spence, D. Starodub, L. Strüder, J. Thøgersen, M. J. J. Vrakking, G. Weidenspointner, T. A. White, C. Wunderer, G. Meijer, J. Ullrich, H. Stapelfeldt, D. Rolles, and H. N. Chapman, “X-ray diffraction from isolated and strongly aligned gas-phase molecules with a free-electron laser,” *Phys. Rev. Lett.* **112**, 083002 (2014).
- <sup>3</sup>J. M. Glowina, A. Natan, J. P. Cryan, R. Hartsock, M. Kozina, M. P. Minitti, S. Nelson, J. Robinson, T. Sato, T. van Driel, G. Welch, C. Weninger, D. Zhu, and P. H. Bucksbaum, “Self-referenced coherent diffraction x-ray movie of ångstrom- and femtosecond-scale atomic motion,” *Phys. Rev. Lett.* **117**, 153003 (2016).
- <sup>4</sup>M. Dantus, S. B. Kim, J. C. Williamson, and A. H. Zewail, “Ultrafast electron diffraction. 5. Experimental time resolution and applications,” *J. Phys. Chem.* **98**, 2782–2796 (1994).
- <sup>5</sup>A. H. Zewail and J. M. Thomas, *Electron Microscopy: Imaging in Space and Time* (Imperial College Press, 2010).
- <sup>6</sup>H. Ihee, V. A. Lobastov, U. M. Gomez, B. M. Goodson, R. Srinivasan, C.-Y. Ruan, and A. H. Zewail, “Direct imaging of transient molecular structures with ultrafast diffraction,” *Science* **291**, 458–463 (2001).
- <sup>7</sup>P. Reckenthaeler, M. Centurion, W. Fuß, S. A. Trushin, F. Krausz, and E. E. Fill, “Time-resolved electron diffraction from selectively aligned molecules,” *Phys. Rev. Lett.* **102**, 213001 (2009).
- <sup>8</sup>B. J. Siwick, J. R. Dwyer, R. E. Jordan, and R. J. D. Miller, “An atomic-level view of melting using femtosecond electron diffraction,” *Science* **302**, 1382–1385 (2003).
- <sup>9</sup>J. Yang, M. Guehr, T. Vecchione, M. S. Robinson, R. Li, N. Hartmann, X. Shen, R. Coffee, J. Corbett, A. Fry, K. Gaffney, T. Gorkhover, C. Hast, K. Jobe, I. Makasyuk, A. Reid, J. Robinson, S. Vetter, F. Wang, S. Weathersby, C. Yoneda, M. Centurion, and X. Wang, “Diffractive imaging of a rotational wavepacket in nitrogen molecules with femtosecond mega-electronvolt electron pulses,” *Nat. Commun.* **7**, 11232 (2016).
- <sup>10</sup>J. Yang, M. Guehr, T. Vecchione, M. S. Robinson, R. Li, N. Hartmann, X. Shen, R. Coffee, J. Corbett, A. Fry, K. Gaffney, T. Gorkhover, C. Hast, K. Jobe, I. Makasyuk, A. Reid, J. Robinson, S. Vetter, F. Wang, S. Weathersby, C. Yoneda, X. Wang, and M. Centurion, “Femtosecond gas phase electron diffraction with MeV electrons,” *Faraday Discuss.* **194**, 563–581 (2016).
- <sup>11</sup>X. Shen, J. P. F. Nunes, J. Yang, R. K. Jobe, R. K. Li, M.-F. Lin, B. Moore, M. Niebuhr, S. P. Weathersby, T. J. A. Wolf, C. Yoneda, M. Guehr, M. Centurion, and X. J. Wang, “Femtosecond gas-phase mega-electron-volt ultrafast electron diffraction,” *Struct. Dyn.* **6**, 054305 (2019).
- <sup>12</sup>T. J. A. Wolf, D. M. Sanchez, J. Yang, R. M. Parrish, J. P. F. Nunes, M. Centurion, R. Coffee, J. P. Cryan, M. Gühr, K. Hegazy, A. Kirrander, R. K. Li, J. Ruddock, X. Shen, T. Vecchione, S. P. Weathersby, P. M. Weber, K. Wilkin, H. Yong, Q. Zheng, X. J. Wang, M. P. Minitti, and T. J. Martínez, “The photochemical ring-opening of 1,3-cyclohexadiene imaged by ultrafast electron diffraction,” *Nat. Chem.* **11**, 504–509 (2019).
- <sup>13</sup>M. Meckel, D. Comtois, D. Zeidler, A. Staudte, D. Pavicic, H. C. Bandulet, H. Pépin, J. C. Kieffer, R. Dörner, D. M. Villeneuve, and P. B. Corkum, “Laser-induced electron tunneling and diffraction,” *Science* **320**, 1478–1482 (2008).
- <sup>14</sup>T. Zuo, A. D. Bandrauk, and P. B. Corkum, “Laser-induced electron diffraction: A new tool for probing ultrafast molecular dynamics,” *Chem. Phys. Lett.* **259**, 313–320 (1996).
- <sup>15</sup>P. B. Corkum, “Plasma perspective on strong field multiphoton ionization,” *Phys. Rev. Lett.* **71**, 1994–1997 (1993).
- <sup>16</sup>Z. Chen, A.-T. Le, T. Morishita, and C. D. Lin, “Quantitative rescattering theory for laser-induced high-energy plateau photoelectron spectra,” *Phys. Rev. A* **79**, 033409 (2009).
- <sup>17</sup>M. Okunishi, T. Morishita, G. Prümper, K. Shimada, C. D. Lin, S. Watanabe, and K. Ueda, “Experimental retrieval of target structure information from laser-induced rescattered photoelectron momentum distributions,” *Phys. Rev. Lett.* **100**, 143001 (2008).
- <sup>18</sup>J. Xu, Z. Chen, A.-T. Le, and C. D. Lin, “Self-imaging of molecules from diffraction spectra by laser-induced rescattering electrons,” *Phys. Rev. A* **82**, 033403 (2010).
- <sup>19</sup>C. D. Lin, A.-T. Le, C. Jin, and H. Wei, “Elements of the quantitative rescattering theory,” *J. Phys. B: At. Mol. Phys.* **51**, 104001 (2018).
- <sup>20</sup>C. D. Lin, A.-T. Le, Z. Chen, T. Morishita, and R. Lucchese, “Strong-field rescattering physics—Self-imaging of a molecule by its own electrons,” *J. Phys. B: At. Mol. Opt. Phys.* **43**, 122001 (2010).
- <sup>21</sup>C. D. Lin, A.-T. Le, C. Jin, and H. Wei, *Attosecond and Strong-Field Physics: Principles and Applications* (Cambridge University Press, 2018).
- <sup>22</sup>C. I. Blaga, J. Xu, A. D. Dichiara, E. Sistrunk, K. Zhang, P. Agostini, T. A. Miller, L. F. Dimauro, and C. D. Lin, “Imaging ultrafast molecular dynamics with laser-induced electron diffraction,” *Nature* **483**, 194–197 (2012).
- <sup>23</sup>M. G. Pullen, B. Wolter, A.-T. Le, M. Baudisch, M. Sclafani, H. Pires, C. D. Schröter, J. Ullrich, R. Moshhammer, T. Pfeifer, C. D. Lin, and J. Biegert, “Influence of orbital symmetry on diffraction imaging with rescattering electron wave packets,” *Nat. Commun.* **7**, 11922 (2016).
- <sup>24</sup>B. Wolter, M. G. Pullen, A.-T. Le, M. Baudisch, K. Doblhoff-Dier, A. Senftleben, M. Hemmer, C. D. Schröter, J. Ullrich, T. Pfeifer, R. Moshhammer, S. Gräfe, O. Vendrell, C. D. Lin, and J. Biegert, “Ultrafast electron diffraction imaging of bond breaking in di-ionized acetylene,” *Science* **354**, 308–312 (2016).
- <sup>25</sup>K. Amini, M. Sclafani, T. Steinle, A.-T. Le, A. Sanchez, C. Müller, J. Steinmetzer, L. Yue, J. R. Martínez Saavedra, M. Hemmer, M. Lewenstein, R. Moshhammer, T. Pfeifer, M. G. Pullen, J. Ullrich, B. Wolter, R. Moszynski, F. J.

- García de Abajo, C. D. Lin, S. Gräfe, and J. Biegert, "Imaging the Renner–Teller effect using laser-induced electron diffraction," *Proc. Natl. Acad. Sci. U. S. A.* **116**, 8173–8177 (2019).
- <sup>26</sup>X. Liu, K. Amini, T. Steinle, A. Sanchez, M. Shaikh, B. Belsa, J. Steinmetzer, A.-T. Le, R. Moshhammer, T. Pfeifer, J. Ullrich, R. Moszynski, C. D. Lin, S. Gräfe, and J. Biegert, "Imaging an isolated water molecule using a single electron wave packet," *J. Chem. Phys.* **151**, 024306 (2019).
- <sup>27</sup>B. Belsa, K. Amini, X. Liu, A. Sanchez, T. Steinle, J. Steinmetzer, A. T. Le, R. Moshhammer, T. Pfeifer, J. Ullrich, R. Moszynski, C. D. Lin, S. Gräfe, and J. Biegert, "Laser-induced electron diffraction of the ultrafast umbrella motion in ammonia," *Struct. Dyn.* **8**, 014301 (2021).
- <sup>28</sup>A. Sanchez, K. Amini, S.-J. Wang, T. Steinle, B. Belsa, J. Danek, A. T. Le, X. Liu, R. Moshhammer, T. Pfeifer, M. Richter, J. Ullrich, S. Gräfe, C. D. Lin, and J. Biegert, "Molecular structure retrieval directly from laboratory-frame photoelectron spectra in laser-induced electron diffraction," *Nat. Commun.* **12**, 1520 (2021).
- <sup>29</sup>Y. Ito, C. Wang, A.-T. Le, M. Okunishi, D. Ding, C. D. Lin, and K. Ueda, "Extracting conformational structure information of benzene molecules via laser-induced electron diffraction," *Struct. Dyn.* **3**, 034303 (2016).
- <sup>30</sup>Y. Ito, R. Carranza, M. Okunishi, R. R. Lucchese, and K. Ueda, "Extraction of geometrical structure of ethylene molecules by laser-induced electron diffraction combined with *ab initio* scattering calculations," *Phys. Rev. A* **96**, 053414 (2017).
- <sup>31</sup>L. Schäfer, "Electron diffraction as a tool of structural chemistry," *Appl. Spectrosc.* **30**, 123–149 (1976).
- <sup>32</sup>P. D. McCaffrey, J. K. Dewhurst, D. W. H. Rankin, R. J. Mawhorter, and S. Sharma, "Interatomic contributions to high-energy electron-molecule scattering," *J. Chem. Phys.* **128**, 204304 (2008).
- <sup>33</sup>S. L. Hinchley, D. A. Wann, and D. W. H. Rankin, "Structure by theory and experiment: One nationality, two languages," *Int. J. Quantum Chem.* **101**, 878–884 (2005).
- <sup>34</sup>E. T. Karamatskos, G. Goldsztejn, S. Raabe, P. Stammer, T. Mullins, A. Trabattoni, R. R. Johansen, H. Stapelfeldt, S. Trippel, M. J. J. Vrakking, J. Küpper, and A. Rouzée, "Atomic-resolution imaging of carbonyl sulfide by laser-induced electron diffraction," *J. Chem. Phys.* **150**, 244301 (2019).
- <sup>35</sup>J. Xu, C. I. Blaga, K. Zhang, Y. H. Lai, C. D. Lin, T. A. Miller, P. Agostini, and L. F. Dimauero, "Diffraction using laser-driven broadband electron wave packets," *Nat. Commun.* **5**, 4635 (2014).
- <sup>36</sup>A.-T. Le, R. R. Lucchese, S. Tonzani, T. Morishita, and C. D. Lin, "Quantitative rescattering theory for high-order harmonic generation from molecules," *Phys. Rev. A* **80**, 013401 (2009).
- <sup>37</sup>G. G. Paulus, W. Becker, W. Nicklich, and H. Walther, "Rescattering effects in above-threshold ionization: A classical model," *J. Phys. B: At., Mol. Opt. Phys.* **27**, L703–L708 (1994).
- <sup>38</sup>X. M. Tong, Z. X. Zhao, and C. D. Lin, "Theory of molecular tunneling ionization," *Phys. Rev. A* **66**, 033402 (2002).
- <sup>39</sup>R. D. Johnson III, NIST Computational Chemistry Comparison and Benchmark Database Number 101 Release 21 August 2020, available at <http://cccbdb.nist.gov/>.
- <sup>40</sup>L. Gagliardi, G. Orlandi, F. Bernardi, A. Cembran, and M. Garavelli, "A theoretical study of the lowest electronic states of azobenzene: The role of torsion coordinate in the cis–trans photoisomerization," *Theor. Chem. Acc.* **111**, 363 (2004).
- <sup>41</sup>D. L. Carroll, FORTRAN genetic algorithm driver (version 1.7a), 2001.
- <sup>42</sup>D. E. Goldberg, *Genetic Algorithms in Search, Optimization, and Machine Learning*, 1st ed. (Addison-Wesley Longman Publishing Co., Inc., 1989).
- <sup>43</sup>R. Srinivasan, V. A. Lobastov, C.-Y. Ruan, and A. H. Zewail, "Ultrafast electron diffraction (UED) a new development for the 4D determination of transient molecular structures," *Helv. Chim. Acta* **86**, 1761–1799 (2003).
- <sup>44</sup>R. L. Dekock and H. B. Gray, *Chemical Structure and Bonding* (University Science Books, 1989), Vol. 229.
- <sup>45</sup>G. Herzberg, *Molecular Spectra and Molecular Structure III: Electronic Spectra and Electronic Structure of Polyatomic Molecules* (Van Nostrand, Inc.; Princeton University Press, 1966).
- <sup>46</sup>H. Fuest, Y. H. Lai, C. I. Blaga, K. Suzuki, J. Xu, P. Rupp, H. Li, P. Wnuk, P. Agostini, K. Yamazaki, M. Kanno, H. Kono, M. F. Kling, and L. F. DiMauro, "Diffractive imaging of C<sub>60</sub> structural deformations induced by intense femtosecond midinfrared laser fields," *Phys. Rev. Lett.* **122**, 053002 (2019).
- <sup>47</sup>B. Wolter, M. G. Pullen, M. Baudisch, M. Sclafani, M. Hemmer, A. Senfleben, C. D. Schröter, J. Ullrich, R. Moshhammer, and J. Biegert, "Strong-field physics with mid-IR fields," *Phys. Rev. X* **5**, 021034 (2015).
- <sup>48</sup>A. Sugita, M. Mashino, M. Kawasaki, Y. Matsumi, R. Bersohn, G. Trott-Kriegeskorte, and K.-H. Gericke, "Effect of molecular bending on the photodissociation of OCS," *J. Chem. Phys.* **112**, 7095–7101 (2000).
- <sup>49</sup>A. G. Császár, G. Czakó, T. Furtenbacher, J. Tennyson, V. Szalay, S. V. Shirin, N. F. Zobov, and O. L. Polyansky, "On equilibrium structures of the water molecule," *J. Chem. Phys.* **122**, 214305 (2005).